Design of Selective Eglin Inhibitors of HCV NS3 Proteinase

Franck Martin,[‡] Nazzareno Dimasi,[‡] Cinzia Volpari,[‡] Claudia Perrera,[‡] Stefania Di Marco,[‡] Mirko Brunetti,[§] Christian Steinkühler,[§] Raffaele De Francesco,[§] and Maurizio Sollazzo*,[‡]

Departments of Protein Engineering & Biocrystallography and Biochemistry, Istituto di Ricerche di Biologia Molecolare (IRBM) P. Angeletti, Via Pontina Km 30,600, 00040 Roma, Italy

Received February 4, 1998; Revised Manuscript Received May 11, 1998

ABSTRACT: Hepatitis C virus (HCV) infection is a major health problem that leads to cirrhosis and hepatocellular carcinoma in a substantial number of infected individuals, estimated to be 100−200 million worldwide. Unfortunately, immunotherapy or other effective treatments for HCV infection are not yet available, and interferon administration has limited efficacy. Different approaches to HCV therapy are being explored, and these include inhibition of the viral proteinase, helicase, and RNA-dependent RNA polymerase and development of a vaccine. Here we present the design of selective inhibitors with nanomolar potencies of HCV NS3 proteinase based on eglin c. These eglin c mutants were generated by reshaping the inhibitor active site-binding loop, and the results emphasize the role played by residues P5−P4′ in enzyme recognition. In addition, alanine scanning experiments provide evidence that the N terminus of eglin c also contributes to NS3 binding. These eglin inhibitors offer a unique tool for accurately assessing the requirements for effective inhibition of the enzymatic activity of NS3 and at the same time can be considered lead compounds for the identification of other NS3 inhibitors in targeted design efforts.

The prevalence of hepatitis C virus (HCV),[1] the major etiological agent of non-A non-B hepatitis (*1*, *2*), is estimated to infect 100−200 million people worldwide. Infection in a very high percentage of cases leads to cirrhosis, hepatocellular carcinoma, and liver failure (*3*). The only available treatment is α-interferon, which provides a sustained response in only about 20% of patients (*4*). Because of the magnitude of this disease and the lack of adequate clinical treatment, our knowledge of viral targets that can lead to the development of effective antivirals needs to be expanded. Approaches to HCV therapy include inhibition of the viral proteinase, helicase, and RNA-dependent RNA polymerase functions, the internal ribosome entry site, and the development of protective immunotherapy. The HCV virion has a positive-strand RNA genome of about 9.4 kb with a single open reading frame encoding a polyprotein of about 3000 amino acids. The polyprotein is processed by cellular and viral factors to become the mature proteins (for a review, see ref *5*). The proteolytic cleavage at the NS3−NS4A, NS4A−NS4B, NS4B−NS5A, and NS5A−NS5B junctions is mediated by a virus-encoded serine proteinase, contained within the 180 N-terminal amino acids of NS3 (*5*). Peptide bond hydrolysis mediated by this proteinase occurs preferentially between C and S or C and A in the substrates cleaved in trans and between T and S in the cis event occurring at the NS3−NS4A junction (*6*). In addition to the NS3 serine proteinase, the NS4A protein is required for efficient cleavage (*7*−*9*). The X-ray structure of the NS3 proteinase 20 kDa domain has been determined as both an apoprotein devoid of cofactor (*10*) and complexed with the NS4A peptide (*11*). These studies have confirmed that the NS3 proteinase domain has a trypsin-like β-barrel fold and that NS4A is an integral component of the fold. It is predicted that inhibition of the NS3 proteinase activity will lead to the production of noninfectious viral particles, thus making this enzyme a favorite target for anti-HCV drug development.

With the aim of generating tools and studying the subsite specificity of the enzyme active site, we recently generated a panel of macromolecule inhibitors of NS3 proteinase using affinity selection strategies (*12*, *13*). Although fairly specific, these inhibitors turned out to have modest potency. To understand whether this was a limitation of the approach, or a feature of the target enzyme, we have attempted the rational design of inhibitors based on eglin c.

Eglin c, which was isolated from *Hirudo medicinalis* (leech), is a very potent inhibitor of several serine proteinases such as *Streptomyces griseus* proteinases A and B, α-chymotrypsin, chymase, and subtilisin (*14*). It is a 70-amino acid inhibitor lacking disulfides but with a remarkably high resistance to acid and thermal denaturation (*15*). The gene encoding eglin c has been synthesized and expressed in *Escherichia coli* (*16*, *17*). The inhibitor belongs to the potato I inhibitor family which includes the closely related barley seed inhibitors CI-1 and CI-2 (*18*). The so-called "standard mechanism", based on a kinetic mechanism of inhibition, was postulated and is valid for most of these serine proteinase

* To whom correspondence should be addressed. Phone: 39-6/91093-222. Fax: 39-6/91093-654. E-mail: Sollazzo@IRBM.IT.

[‡] Department of Protein Engineering & Biocrystallography.

[§] Department of Biochemistry.

[1] Abbreviations: BPTI, bovine pancreatic trypsin inhibitor; CHAPS, 3-(3-cholamidopropyl)dimethylammonio-1-propanesulfonate; CI-1 and CI-2, chymotrypsin inhibitor 1 and 2, respectively; CD, circular dichroism; DTT, dithiothreitol; EDTA, ethylenediaminetetraacetic acid; HEPES, *N*-(2-hydroxyethyl)piperazine-*N*′-2-ethanesulfonic acid; HCV, hepatitis C virus; HLE, human leukocyte elastase; HPLC, high-pressure liquid chromatography; NMR, nuclear magnetic resonance; PAGE, polyacrylamide gel electrophoresis; PCR, polymerase chain reaction; R_H, hydrodynamic radius; RP, reversed-phase; $T_{m(r)}$, relative melting temperature; TFA, trifluoroacetic acid; TB, tryptone broth.

S0006-2960(98)00283-9 CCC: $15.00
Published on Web 08/01/1998

inhibitors (*18*, *19*). By virtue of this mechanism, the inhibitor binds with its substrate-like region (active site-binding loop) at the enzyme active site. Generally, the active site-binding loop of serine proteinase inhibitors is held in its conformation either by covalent interactions with the rest of the molecule formed by disulfide bridges, as in basic pancreatic trypsin inhibitor (BPTI) (*20*), or by noncovalent interactions, as found in the inhibitors of the potato I inhibitor family (*21*). The structure of uncomplexed eglin c has been determined by both two-dimensional NMR (*22*) and X-ray crystallography (*23*). In addition, the crystal structures of eglin c in complex with subtilisin (*24*−*27*), α-chymotrypsin (*28*), and thermitase (*29*) have also been solved. The tertiary structure of eglin c (Figure 1A) consists of a hydrophobic core and an exposed proteinase binding loop (residues 40−48). The hydrophobic core contains a twisted four-stranded β-sheet and a short α-helix (residues 18−25). The active site-binding loop with the scissile bond between L^{45} (P1) and D^{46} (P1′) is held in its conformation by electrostatic and hydrogen bond interactions involving T^{44} (P2) and D^{46} (P1′) of the binding loop, R^{51} and R^{53} of the "hydrophobic core", and the C terminus of G^{70}. X-ray crystallography and mutagenesis studies of P1 residues (*30*−*32*) have shown that the specificity of enzyme−inhibitor complex formation is determined by the substrate binding pockets (usually S3−S3′) of the proteinase and the corresponding residues of the inhibitor (P3−P3′). Here we have applied this knowledge to design a panel of selective eglin inhibitors of NS3 proteinase with nanomolar potencies by reshaping the active site-binding loop and also provide evidence that the N terminus of eglin c contributes to NS3 binding.

EXPERIMENTAL PROCEDURES

Microbiological and Recombinant DNA Techniques. Microbiological and recombinant DNA techniques were employed according to standard protocols or as recommended by suppliers. The polymerase chain reaction (PCR) primers used to create the eglin c gene were the same as described before (*17*), except that two different restriction enzyme sites were designed at the 5′ (*Nde*I) and 3′ (*Hin*dIII) ends for cloning into the pT7 vector. We also introduced a *Sma*I site in the eglin gene which produced a deletion of the region encoding the active site-binding loop. Eglin mutants were generated by introducing double-stranded oligonucleotides encoding the desired loop sequence in the *Sma*I-digested vector. To construct the alanine scanning mutants at the NH_2 terminus of the inhibitor, we used PCR amplification of eglin c gene with appropriate primer pairs and products were digested with *Nde*I and *Hin*dIII and subcloned into the same sites of the pT7 vector. Nucleotide sequences were determined using Sequenase (U.S. Biochemical Corp., Cleveland, OH) according to the supplier's recommendations. The protein concentration was determined by quantitative amino acid analysis.

Eglin Purification. The eglin variants were expressed from BL21 *E. coli* cells transformed with pT7-driven vectors. The cultures were grown at 37 °C in tryptone broth (TB) medium in shaking flasks. Protein production was induced when the OD_{600nm} reached 2.0 by addition of 400 μM isopropyl β-D-thiogalactopyranoside, and culture growth was continued for 3 h. This procedure yields 20−100 mg of protein per liter of culture. The pellet corresponding to 500 mL of culture was resuspended in 25 mL of lysis buffer containing 50 mM Tris-HCl (pH 8.0), 1 mM ethylenediaminetetraacetic acid (EDTA), and 5 mM dithiothreitol (DTT) and submitted to 20 cycles of microfluidizer at 40 psi (Microfluidics Corp.). The lysate was centrifuged, and the supernatant was made 2% with acetic acid and kept on ice for 20 min. After centrifugation, the pH of the soluble fraction was adjusted to 8.0 and the sample concentrated to 5 mL in an Amicon ultrafiltration device. The sample was then loaded at 2 mL/min on a Superdex 75 preparation grade column equilibrated

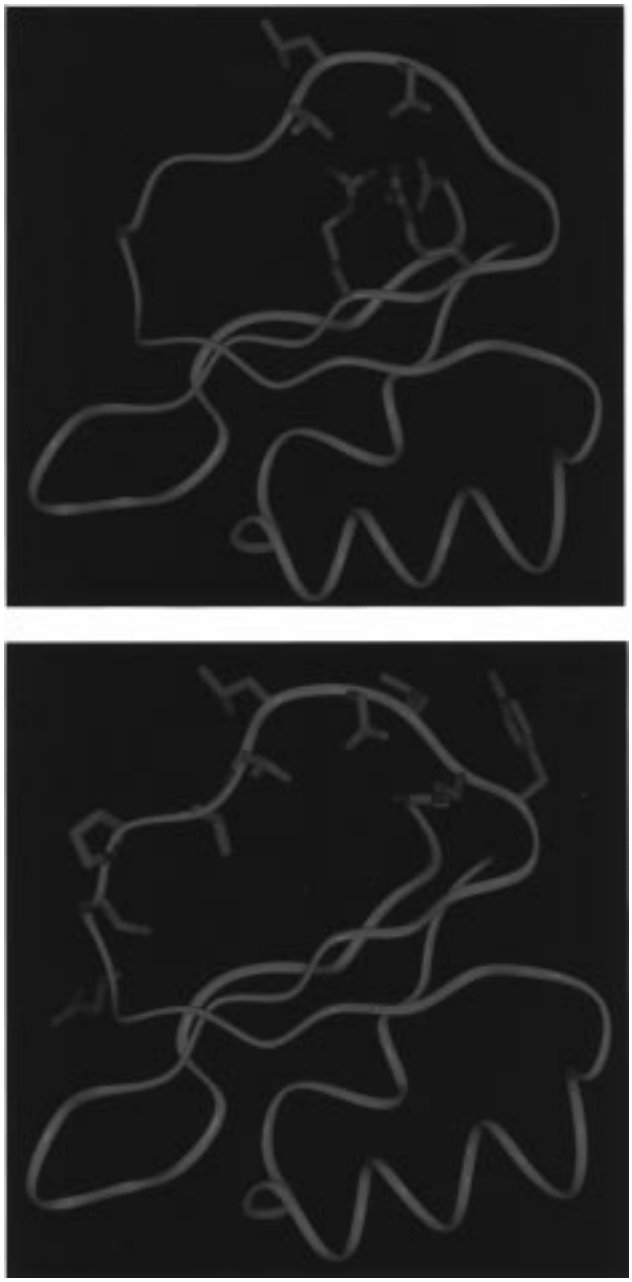

FIGURE 1: Eglin c structure. (A, top) The cartoon diagram of the inhibitor was drawn using the atomic coordinates of the eglin c−mesentericopeptidase complex obtained from the Brookhaven National Laboratory Protein Data Bank (1MME). The flexible N terminus (residues 1−7) is absent; side chains of active site loop-stabilizing (T^{44}, D^{46}, R^{51}, R^{53}) and P1 (L^{45}) residues and the C terminus are shown. (B, bottom) The side chains of the active site-binding loop encompassing residues 39−49 (from left to right) corresponding to P6−P4′ that were mutagenized are shown.

in 20 mM carbonate buffer containing 5 mM DTT. Fractions corresponding to eglin were collected and tested for purity on Tris-tricine SDS−polyacrylamide gels (PAGE).

Purification of the NS3 Proteinase Domain. Expression and purification were performed as described previously (*33*). The protein concentration was estimated by quantitative amino acid analysis. The purity of the enzyme was checked on silver-stained SDS−PAGE and by reversed-phase (RP) high-pressure liquid chromatography (HPLC) using a Vydac C4 column (4.6 mm × 250 mm, 5 μm, 300 Å). Eluents were H_2O/0.1% trifluoroacetic acid (TFA) (buffer A) and acetonitrile/0.1% TFA (buffer B). A linear gradient from 3 to 95% B over the course of 60 min was used.

Synthetic Peptides for the HPLC Assay. Our standard substrate was a 13-amino acid synthetic peptide derived from the cleavage sequence of the NS4A−NS4B junction (Ac-DEEMECASHLPYK-NH_2). As proteinase cofactor, we used a 14-mer peptide corresponding to the central hydrophobic core of the NS4A protein spanning residues 21−34 (pep4A, Ac-KKKGSVVIVGRIILSGR-NH_2). After cleavage and deprotection, the crude peptides were purified by RP-HPLC to >98% purity. The identity of peptides was checked by mass spectrometry, and their concentration was determined by quantitative amino acid analysis performed on HCl-hydrolyzed samples. Stock solutions of peptides, prepared in dimethyl sulfoxide, were kept at −80 °C until use.

NS3 Proteinase Assays. Assays were performed in 50 mM *N*-(2-hydroxyethyl)piperazine-*N*′-2-ethanesulfonic acid (HEPES, pH 7.5), 1% 3-(3-cholamidopropyl)dimethylammonio-1-propanesulfonate (CHAPS), 15% glycerol, 30 mM DTT, and 15 μM pep4A, using 1−20 nM recombinant purified NS3. The IC_{50} values were calculated by fitting inhibition data to eq 1 using Kaleidagraph software:

$$\% \text{ activity} = (\text{maximum activity})/[1 + ([I]/IC_{50})^S] \quad (1)$$

where [I] is the eglin concentration, maximum activity is that of the enzyme in the absence of inhibitor, and S is the slope factor of the curve. Inhibition mechanisms were determined by performing substrate titration experiments (*12*, *13*). Double-reciprocal plots ($1/V$ vs $1/S$) were used to visualize inhibition mechanisms. Kinetic parameters were calculated from a least-squares fit of initial rates as a function of substrate concentration using Kaleidagraph or Sigmaplot software, assuming Michaelis−Menten kinetics. The values of the dissociation constants of the enzyme−inhibitor complex (K_i) and of the ternary enzyme−inhibitor−substrate complex (K_{ii}) were calculated by refitting the data to a modified Michaelis−Menten equation (eq 2):

$$V = V_{max}S/[K_m(1 + [I]/K_i) + S(1 + [I]/K_{ii})] \quad (2)$$

Circular Dichroism Spectroscopy. The far-ultraviolet circular dichroism (UV-CD) spectra of the purified proteins were measured with a Jasco J-710 spectropolarimeter using a quartz cell with a path length of 0.1 cm. Each measurement was the average of five repeated scans in steps of 10 nm at 23 °C. The samples were measured at a protein concentration of 13 μM in 10 mM phosphate buffer (pH 7.5) and 0.1 mM DTT. For the temperature scan, the wavelength was set at 197 nm, with a step resolution of 0.1 °C. The temperature range varied between 40 and 90 °C with a temperature slope of 10 °C/h.

Stoichiometry Determination. Equivalence titration was performed to determine equimolar amounts of NS3 serine proteinase−inhibitor pairs. Eglin mutants at increasing concentrations were incubated with a fixed concentration of NS3 proteinase that was 5-fold higher than the inhibitor IC_{50}. As for the NS3 assay, samples were preincubated for 15 min and reaction was started with the addition of 20 μM substrate and stopped with a 1% TFA solution after incubation for 40 s. The percentage of NS3 residual activity, determined by HPLC assay, was plotted versus the inhibitor concentration, and a linear curve was fitted. The intersection of the extrapolated curve with the abscissa corresponds to the amount of inhibitor necessary to saturate the enzyme.

Dynamic Light Scattering. Light scattering was performed with a Dynapro-801 Molecular Sizing Instrument with temperature control (Protein Solutions, Inc., Charlottesville, VA). Data analyses were performed on Protein Solutions' Dynamics analysis software. The purified proteins in solution were injected through 0.1 μm syringe filters at 20 °C into the Dynapro-801 detector, which uses a solid state laser (20 mW power) to illuminate the sample with 780 nm light in a 7 μL quartz flow cell. The ternary complex NS3−pep4A cofactor−eglin mutants (1:1:1 molar ratio) were evaluated at protein concentrations of 115 μM in 50 mM sodium acetate buffer (pH 6.5) containing 250 mM NaCl, 10% glycerol, 5 mM DTT, 0.1% (w/v) β-octylglucoside, and 0.02% NaN_3. The complex NS3−pep4A cofactor peptide (1:1 molar ratio) was evaluated at protein concentrations of 130 μM, in the same buffer as above.

Determination of Association Rate Constants. A SX-MV18 Applied Photophysics stopped flow apparatus equipped with a sequential flow device was used to fluorimetrically monitor the NS3-dependent cleavage of the internally quenched fluorogenic depsipeptide substrate DED(EDANS)-EEAbuΨ[COO]ASK(DABCYL) (*34*). The excitation monochromator was set at 355 nm, and a 400 nm cutoff emission filter was used to suppress the excitation light. Rates were measured under pseudo-first-order conditions. Enzyme (30 nM) and substrate (15 μM) were mixed prior to addition of an equal volume of 1−8 μM eglin in 50 mM HEPES (pH 7.5), 15% glycerol, 10 mM DTT, 1% CHAPS, and 30 μM NS4A cofactor peptide. A value of 2 μM was determined for the K_m of NS3-catalyzed hydrolysis of the ester substrate. Data from at least three runs were averaged, and the resulting progress curves were fitted by nonlinear least-squares analysis to eq 3:

$$F = V_s t + (V_o - V_s)[1 - \exp(-k_{obs}t)]/k_{obs} + F_o \quad (3)$$

with F being the measured fluorescence defined as a function of the initial (V_o) and final (V_s) steady state velocities and of the apparent first-order rate constant k_{obs} for the approach of the velocity to its final value and F_o being the initial displacement of F from 0 at $t = 0$. k_{obs} values obtained from the fit were used to calculate the second-order association rate constant k_{on} using eq 4:

$$k_{obs} = k_{off} + k_{on}[[\text{eglin}]/(1 + [S]/K_m)] \quad (4)$$

where [S] is the final substrate concentration and K_m the Michaelis constant for substrate hydrolysis.

Determination of Thermodynamic Parameters of Eglin−Proteinase Complex Formation. Values for the apparent free energy $\Delta G°$ of eglin−NS3 complex formation were calculated from values of K_a obtained at 23 °C. The apparent enthalpy variation $\Delta H°$ was calculated from the linear dependence of log K_a on $1/T$ with van't Hoff plots according to eq 5:

$$\Delta H° = -2.3R[\mathrm{d}(\log K_a)/\mathrm{d}(1/T)] \quad (5)$$

The apparent entropy variation $\Delta S°$ associated with complex formation was calculated at 23 °C from the values of $\Delta G°$ and $\Delta H°$. All data were obtained in 25 mM HEPES (pH 7.5), 15% glycerol, 1% CHAPS, 10 mM DTT, and 16 μM pep4A, using the peptide Ac-DEMEECASHLPYK-NH_2 as substrate. The pH of the buffer was corrected for the temperature effects. Substrate cleavage was monitored by HPLC as described above.

Human Leukocyte Elastase Activity Assay. The human leukocyte elastase (HLE) was purchased from Worthington Biochemical Corp., and its substrate (Me-*o*-Suc-Ala-Ala-Pro-Val-pNA) from Calbiochem. The HLE assay was performed in a 96-well plate, in 100 mM Tris-HCl buffer (pH 7.5), 500 mM NaCl, 0.5% Triton X-100, and 30 mM DTT. The enzyme and the substrate were added to final concentrations of 20 nM and 120 μM, respectively. Samples were tested in triplicate in a 100 μL final volume, and after incubation for 75 min at room temperature under constant agitation, the OD was recorded at 405 nm.

GB Virus B Proteinase Inhibition Assay. The purified GBV-B NS3 proteinase was a kind gift from C. Traboni (IRBM). The assay was performed using the same protocol that was used for the HCV NS3 proteinase, in the following buffer: 50 mM HEPES (pH 7.5), 30% glycerol, 30 mM DTT, 2% CHAPS, and 25 nM proteinase. The substrate concentration used was 50 μM ($6.3 \times K_m$).

RESULTS

Rationale and Experimental Strategy. The strategy used to design the NS3 inhibitors derived from eglin c was based on the assumption that upon reshaping its surface properties, by virtue of its conformation, the eglin binding loop (Figure 1B) would provide tight binding to the NS3 enzyme. The main reason for choosing eglin c, rather than other macromolecule scaffolds, was its lack of disulfide bonds. Because of this property, eglin c is amenable to high levels of expression in the cytoplasm of *E. coli* and can withstand (without undesirable consequences) the experimental reducing conditions required for optimal proteinase activity. To engineer our inhibitor series, we assembled an eglin c synthetic gene for expression in *E. coli*. The purified protein analyzed by mass spectrometry shows two components: the main component having M^1 removed and the N terminus acetylated and the minor component (2%) having nonacetylated M^1 as the N-terminal residue. Wild-type eglin c and P1 mutant C^{45} eglin c (egl-*C1*) did not inhibit NS3 proteinase activity up to the maximal concentration tested of 180 μM (Table 1).

Design, Partial Optimization, and the Role of P5−P4′ Residues. Two series of inhibitors were designed on the basis of NS4A/4B (Table 1, panel A) and NS5A/5B (Table 1, panel B). The first two inhibitors ($E^{41}E^{43}C^{45}$ eglin c and $D^{41}V^{42}C^{45}$ eglin c, hereafter egl-*EPE* and egl-*W*) of the series were aimed at replacing the minimum number of residues perceived to be essential for binding to the enzyme active site as deduced from the substrate (*35*). At the same time, we wanted to minimize possible alterations to the "optimal" backbone conformation of the active site-binding loop. The mutants egl-*EPE* and egl-*W* were proven to be competitive inhibitors (data not shown) with respective IC_{50} values of 0.39 and 2 μM. A number of criteria were established to characterize these and all the following eglin mutants. First, inhibition was determined to be reversible, as more than 90% of the activity was recovered upon dilution of the enzyme−inhibitor complex. This turned out to hold true for all eglin mutants constructed. Second, inhibition was competitive with substrate, indicating active site binding. Third, all eglin mutants were examined by far-UV CD spectroscopy (190−250 nm) and shown not to differ in their secondary structure content with respect to eglin c. Fourth, the relative melting temperature [$T_{m(r)}$] of eglin mutants was determined by monitoring the value of the molar ellipticity at 197 nm as a function of temperature (Table 1). The reversibility of thermal denaturation of all mutants was tested by CD spectroscopy and by determination of the specific activity after renaturation. Since the NS4A/4B-based variant seems more promising than egl-*W* and fulfils all above-mentioned criteria of structural integrity and active site binding, we carried out most of the structure activity relationship experiments in the egl-*EPE* context. To increase the residue similarity between eglin loop variants and the natural proteinase substrate, two other mutants were generated: $E^{41}E^{43}E^{44}C^{45}$ eglin c (egl-*PEE*) and $E^{41}M^{42}E^{43}C^{45}$ eglin c (egl-*EME*). Both mutations produced a potency decrease. Mutation of the P2 residue in egl-*PEE* also correlates with a decrease in protein thermodynamic stability. To characterize the contribution in the loop stabilization of residues other than P2 (such as P6, P1′, and G^{70}), we generated another set of mutants.

The acidic residue that is strictly conserved in all proteinase substrates in the P6 position and demonstrated to be important to the specificity for NS3 proteinase (*18*) could not be easily accommodated in the backbone conformation of the eglin inhibitor. In fact, the eglin c residue G^{40} corresponding to P6 is in a nonallowed conformation of Φ and ψ angles for any residue other than G (*25*). The attempt to introduce the acidic residue at P6, and concurrent shifting of the G residue by one position toward the N terminus in two variants, $G^{39}D^{40}E^{41}E^{43}E^{44}C^{45}$ eglin c (egl-*GD*) and $G^{39}D^{40}E^{41}M^{42}E^{43}E^{44}C^{45}$ eglin c (egl-*GP*), resulted in a considerable loss of potency with a simultaneous decrease in thermodynamic stability [compare the $T_{m(r)}$ values of egl-*GD* and egl-*GP* with that of egl-*PEE*]. The next residue contribution to be assessed was the P1′ aspartic acid which was changed to glutamic acid in the $E^{41}M^{42}E^{43}C^{45}E^{46}$ eglin c variant (egl-*P1′*). This mutation affects protein stability and at the same time the inhibitor potency. Finally, the role of the C terminus of eglin c G^{70}, previously recognized as an important structural determinant of the active site-binding loop (*25*), was investigated in the context of both inhibitor series. The C terminus of egl-*EME* and of egl-*W* was replaced with the carboxyl group of an D side chain, and an additional G residue at the C terminus of the molecules was inserted ($D^{70}G^{71}$ double mutants, hereafter named egl-*EMEG70* and egl-*WG70*). This design was also described

Table 1: Eglin Inhibitors of NS3[a]

Panel	eglin variant		P_6	P_5	P_4	P_3	P_2	P_1	$P_{1'}$	$P_{2'}$	$P_{3'}$	$P_{4'}$	[§]$Tm_{(r)}$ ±1 (°C)	IC_{50}±10% (μM)
		39	40	41	42	43	44	45	46	47	48	49		
	eglin c	E	G	S	P	V	T	L	D	L	R	Y	84	not active
A	egl-*ELEMS*	E	G	E	L	E	T	C	D	M	S	Y	79	0.06
	egl-*EPEMS*	E	G	E	P	E	T	C	D	M	S	Y	78	0.18
	egl-*EMEMS*	E	G	E	M	E	T	C	D	M	S	Y	78	0.20
	egl-*ELE*	E	G	E	L	E	T	C	D	L	R	Y	84	0.26
	egl-*ELEMSL*	E	G	E	L	E	T	C	D	M	S	L	nd	0.28
	egl-*EPE*	E	G	E	P	E	T	C	D	L	R	Y	80	0.39
	egl-*EME*	E	G	E	M	E	T	C	D	L	R	Y	80	0.5
	egl-*PEE*	E	G	E	P	E	E	C	D	L	R	Y	74	0.6
	egl-*EPEMSΔN*	E	G	E	P	E	T	C	D	M	S	Y	78	1.08
	egl-*P1′*	E	G	E	M	E	T	C	E	L	R	Y	72	1.44
	egl-*ELI*	E	G	E	L	I	T	C	D	L	R	Y	82	1.48
	egl-*KLEMS*	E	G	K	L	E	T	C	D	M	S	Y	nd	4.6
	egl-*T1*	E	G	E	P	E	E	T	D	L	R	Y	74	6.2
	egl-*S1*	E	G	E	P	E	E	S	D	L	R	Y	74	6.9
	egl-*EMEG70*	E	G	E	M	E	T	C	D	L	R	Y	68	7.3
	egl-*V*	E	G	E	M	V	T	C	D	L	R	Y	84	10.6
	egl-*GD*	G	D	E	P	E	E	C	D	L	R	Y	72	17.3
	egl-*GP*	G	D	E	M	E	E	C	D	L	R	Y	72	18.2
	egl-*L1*	E	G	E	L	E	T	L	D	M	S	Y	79	48.1
	egl-*C1*	E	G	S	P	V	T	C	D	L	R	Y	84	not active
	NS4A/4B		D	E	M	E	E	C	A	S	H	L		
B	egl-*WMS*	E	G	D	V	V	T	C	D	M	S	Y	78	1.05
	egl-*DIVMS*	E	G	D	I	V	T	C	D	M	S	Y	nd	1.29
	egl-*W*	E	G	D	V	V	T	C	D	L	R	Y	82	2.0
	egl-*WG70*	E	G	D	V	V	T	C	D	L	R	Y	68	3.1
	egl-*TV*	E	G	D	T	V	T	C	D	L	R	Y	78	5.1
	egl-*YWMS*	E	G	Y	V	V	T	C	D	M	S	Y	nd	12.5
	NS5A/5B		E	D	V	V	C	C	S	M	S	Y		

[a] Amino acid sequences of the engineered eglin active site-binding loops (mutated residues are indicated by shaded cells) and their corresponding $T_{m(r)}$ and IC_{50} values. The mutant nomenclature is defined in the text. The residue number (39−49) and its corresponding position in the active site-binding loop (P6−P4′) are indicated in the top row. Both NS4A/4B and NS5A/5B substrates are aligned at the bottom of each panel. Nonactive molecules were tested at the maximum concentration compatible with the assay, namely 180 μM (20-fold dilution of a 3.6 mM stock solution). nd, not determined. § $T_{m(r)}$ is the relative melting temperature of eglin mutants determined by monitoring the value of circular dichroism (Θ) at 197 nm as a function of temperature, taking as a reference the temperature at which Θ_{197} was halved.

recently on CI-2 inhibitor and shown to be active, albeit at a reduced potency (*36*). All the above mutations were detrimental to the thermodynamic stability of eglin c, the most destabilizing being the $D^{70}G^{71}$ double mutation. Since thermodynamic destabilization is always associated with a loss of potency ranging from 1.5- to 14-fold (compare egl-*EME* with egl-*P1′*, egl-*EPE* with egl-*PEE*, egl-*EME* with egl-*EMEG70*, and egl-*W* with egl-*WG70*), we attempted to increase the thermodynamic stability of the inhibitors. This was achieved by restoring in the egl-*EME* context the native V^{43} residue present both in the eglin c loop and in the NS5A/5B substrate in the P3 position. The resulting molecule $E^{41}M^{42}C^{45}$ eglin c (egl-*V*) was as stable as the wild-type eglin c, but its IC_{50} was higher than that of egl-*EME*, demonstrating the importance of the negative charge at P3. This was further confirmed by the design of $E^{41}L^{42}I^{43}C^{45}$ eglin c (egl-*ELI*).

To confirm the critical role of the P1 residue, additional mutants were constructed. The amino acid at P1 was replaced either with S (sterically and electronically, the most compatible residue) or with T (the alternative P1 residue of the cis-cleaved site at the NS3−NS4A junction). Both $E^{41}E^{43}E^{44}S^{45}$ eglin c (egl-*S1*) and $E^{41}E^{43}E^{44}T^{45}$ eglin c (egl-*T1*) are 1 order of magnitude less potent than the corresponding C^{45} mutant (egl-*PEE*). In addition, when residue C^{45} of the most potent inhibitor $E^{41}L^{42}E^{43}C^{45}M^{47}S^{48}$ eglin c (egl-*ELEMS*, vide infra) is replaced by wild-type residue L ($E^{41}L^{42}E^{43}L^{45}M^{47}S^{48}$ eglin c), the loss of potency is about 3 orders of magnitude (egl-*L1*, Table 1).

Having thus explored the limitations imposed by the structural constraints of the eglin c scaffold, we set out to selectively modify permissive positions in an attempt to optimize contacts with the active site of the NS3 protease. On the basis of the knowledge of the natural substrate NS4A/4B, and of structure−activity relationship studies carried out on synthetic substrates (*35*), another set of mutants was generated to probe L, I, and T residues in P4 position. After analysis of the corresponding inhibitors, the $E^{41}L^{42}E^{43}C^{45}$ eglin c (egl-*ELE*) was shown to be the best compromise between thermodynamic stability and potency.

We then investigated the effect of P2′ and P3′ residue cosubstitution by constructing $E^{41}E^{43}C^{45}M^{47}S^{48}$ eglin c (egl-*EPEMS*), $E^{41}L^{42}E^{43}C^{45}M^{47}S^{48}$ eglin c (egl-*ELEMS*), $E^{41}M^{42}E^{43}C^{45}M^{47}S^{48}$ eglin c (egl-*EMEMS*), and $D^{41}V^{42}C^{45}M^{47}S^{48}$ eglin c (egl-*WMS*). These are the residues of the P′ region of NS5A/5B substrate M (P2′) and S (P3′), respectively, which have higher affinity than NS4A/4B counterparts for the proteinase active site.[2] As a result, these

[2] Our unpublished observations.

mutations improved potency by 2.5−4-fold in all configurations tested (compare egl-*ELEMS*, egl-*EPEMS*, egl-*EMEMS*, and egl-*WMS* with corresponding inhibitors bearing wild-type P′ residues). It should be considered that Y in P4′, present in all inhibitors, is also part of the NS5A/5B substrate, and its contribution to binding was investigated by designing $E^{41}L^{42}E^{43}C^{45}M^{47}S^{48}L^{49}$ eglin c (egl-*ELEMSL*) where Y^{49} was substituted with L. The comparison of egl-*ELEMSL* with egl-*ELEMS* clearly demonstrates that Y^{49} is involved in binding to NS3. Some authors (*37*) have postulated a direct interaction between the NS4A cofactor and the P4′ substrate residue.

Electrostatic rather than hydrophobic interactions appear to dictate specificity and complementarity between the NS3 active site and eglin inhibitors (compare panel A with panel B of Table 1). This is especially evident for residues P3 and P5 which, when mutated to hydrophobic residues, cause a reduction in potency as shown by comparison of egl-*EME* to egl-*V* and $D^{41}V^{42}C^{45}M^{47}S^{48}$ eglin c to $Y^{41}V^{42}C^{45}M^{47}S^{48}$ eglin c (egl-*WMS* and egl-*YWMS*, respectively). In addition, the requirement of a negative charge at P5 is clear, as indicated by the lower potency of $K^{41}L^{42}E^{43}C^{45}M^{47}S^{48}$ eglin c (egl-*KLEMS*) compared to $E^{41}L^{42}E^{43}C^{45}M^{47}S^{48}$ eglin c (egl-*ELEMS*).

Mechanism of Inhibition. To test if the mechanism of inhibition of our series was compatible with a "classical mechanism", we focused on the two most potent inhibitors, egl-*ELEMS* and egl-*EPEMS*, on which substrate titration experiments in the absence and in the presence of different concentrations of the inhibitors were performed (Figure 2). By fitting the experimental data to a modified Michaelis−Menten equation (eq 2), we determined the K_i and K_{ii}. We obtained K_i values of 90 and 30 nM for egl-*EPEMS* and egl-*ELEMS*, respectively, and very large values of K_{ii} for both molecules. This result indicates that both inhibitors bind to the free enzyme but have virtually no affinity for the enzyme−substrate complex, as expected for a competitive inhibitor.

Equivalence titrations were performed to determine the stoichiometry of the NS3 serine proteinase−inhibitor complex (*38*). Inhibitor at increasing concentrations was added to a constant amount of NS3 proteinase (approximately a 5-fold excess over the IC_{50} value of the inhibitor), and subsequently, the residual enzyme activity was determined by HPLC. The equivalence titration curves are shown in Figure 2 (insets) for egl-*ELEMS* and egl-*EPEMS*. The idealized equivalence point, corresponding to the eglin concentration necessary to fully inhibit the proteinase, can be derived at the intersection of the extrapolated inhibition curve with the abscissa. This value was compatible with a 1:1 ratio for both inhibitors, and it was further confirmed by gel filtration (data not shown) and dynamic light scattering studies of the ternary complexes of the NS3/NS4A−inhibitors. The formation of a complex between NS3/NS4A and the eglin mutants was investigated by assuming the proteins to be globular in nature. Molecular size estimation showed that NS3/NS4A, egl-*ELEMS*, and egl-*EPEMS* have hydrodynamic radii (R_H) of 2.5, 1.7, and 1.4 nm, respectively, with a standard deviation of the spread of particle sizes around the reported average radius of 15−20% for all samples. Software-based conversion of R_H measurements

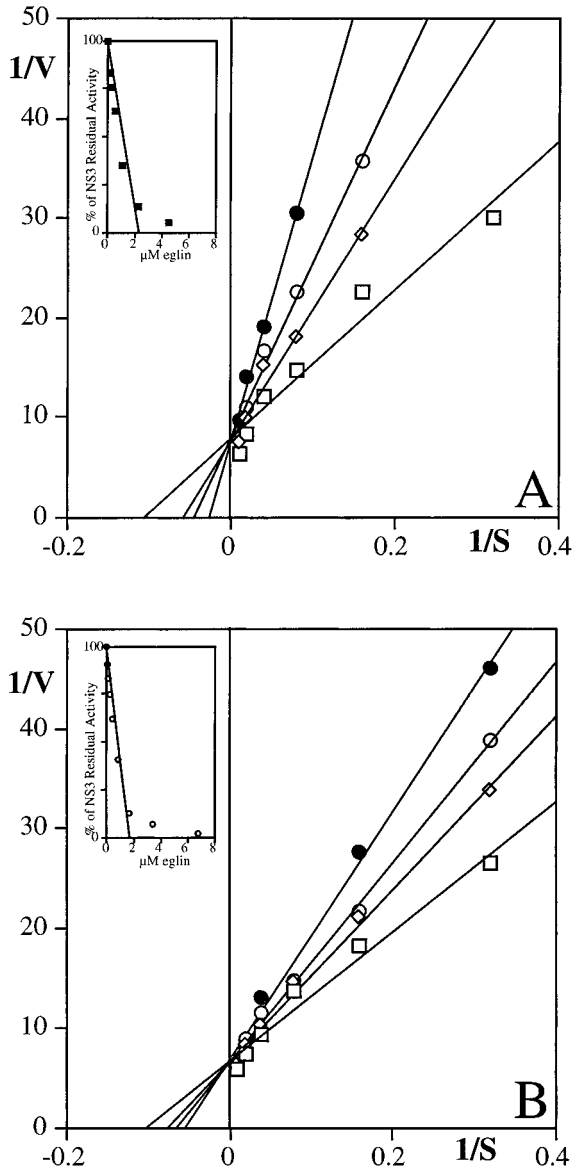

FIGURE 2: Determination of the inhibition mechanism and stoichiometry. Mechanisms of inhibition of NS3 proteinase activity by egl-*EPEMS* and egl-*ELEMS* are shown as Lineweaver−Burk plots (double reciprocal of velocity vs substrate concentration). Substrate titration curves were recorded in the absence of inhibitor (□) and in the presence of 90 (◇), 180 (○), and 360 nM (●) egl-*EPEMS* (A). The same symbols correspond to 0, 30, 60, and 120 nM egl-*ELEMS*, respectively in panel B. Equivalence titration experiments were performed in the presence of 2.5 or 1.5 μM NS3 proteinase for egl-*EPEMS* (squares) and egl-*ELEMS* (circles), and the results are shown in the insets of panels A and B, respectively. The equivalence concentration representing a 1:1 complex was given at the intersection of the extrapolated curves with the abscissa. All experimental points are the mean of duplicate samples.

estimated a molecular mass of 26, 11, 8 kDa for NS3/NS4A, egl-*ELEMS*, and egl-*EPEMS*, respectively. The relatively low percentage of polydispersion (15−20%) indicates that the NS3/NS4A complex and the eglin mutants exist as a homogeneously single monomeric species in solution. After complex formation between NS3/NS4A (115 μM) and 1 equiv of eglin c mutants (corresponding to more than 100-fold excess over the K_D values under these assay conditions), a single species with an R_H of 2.6 nm for both ternary complexes was found (estimated molecular mass of 28 kDa), confirming a 1:1:1 stoichiometry.

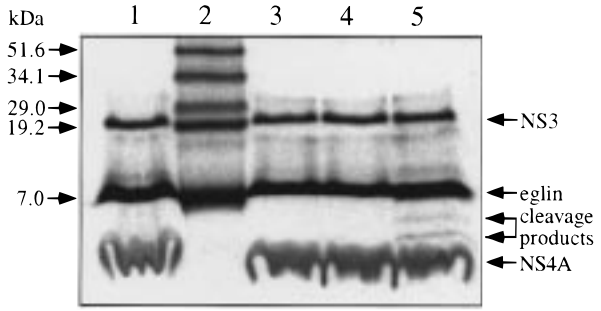

FIGURE 3: Cleavage of eglin mutants by NS3 proteinase. Coomassie-stained SDS−PAGE of egl-*ELEMS*, egl-*PEE*, and egl-*EMEG70* incubated for 16 h in the presence of NS3 proteinase as described in Experimental Procedures (lanes 3−5). Lane 1 corresponds to a sample at time 0 of incubation, and lane 2 shows molecular mass markers.

Table 2: Kinetic Parameters of Binding[a]

inhibitor	k_{on} (M^{-1} s^{-1})	k_{off} (s^{-1})
egl-*EPEMS*	$5.8 \times 10^6 \pm 2.2 \times 10^6$	0.3 ± 0.1
egl-*ELEMS*	$9.6 \times 10^6 \pm 1.8 \times 10^6$	0.9 ± 0.3

[a] Association rate constants in the homogeneous phase for egl-*EPEMS* and egl-*ELEMS* were determined by stopped-flow experiments as described in the text. The dissociation constant (k_{off}) value was derived from the intercept of plots of k_{obs} vs inhibitor concentration.

Thermodynamic Parameters of the Eglin−Proteinase Complex. To gain more insight into the mechanism of inhibition, with respect to the relative entropic and enthalpic contributions to binding energy, we determined the temperature dependence of the inhibition of NS3 proteinase by egl-*ELEMS*. Values for the apparent free energy $\Delta G°$ of inhibitor−NS3−NS4A complex formation (−40 kJ/mol) were calculated from values of K_a obtained at 23 °C. The apparent enthalpy variation $\Delta H°$ (−6.5 kJ/mol) was calculated from the linear dependence of log K_a on $1/T$ with van't Hoff plots according to eq 3. As shown in Figure 4, this thermodynamic analysis indicates that binding of eglin inhibitors to NS3 proteinase is in fact entropy-driven ($T\Delta S$ = 33.5 kJ/mol).

Pre-Steady State Kinetic Parameters of Eglin−Proteinase Complex Formation. Next, we determined the pre-steady state kinetic parameters for the inhibitors. To this end, we monitored the time dependence of the inhibition of a continuously monitored cleavage reaction in the homogeneous phase. As reported in Table 2, the calculated association rate constants of optimized eglin inhibitors are close to the theoretical limits of diffusion rates in solution (10^6−10^7 M^{-1} s^{-1}), suggesting that the encounter between eglin mutants and the NS3 proteinase is diffusion-controlled. The dissociation rate constants are 0.9 and 0.3 s^{-1} for egl-*ELEMS* and egl-*EPEMS* complexes, respectively.

Inhibitor versus Substrate Activity and Selectivity. We wanted to test whether the thermodynamic stability of the inhibitors correlated with the susceptibility to cleavage by the enzyme. The inhibitors egl-*ELEMS* (most stable) and egl-*PEE* (intermediate stability) were not cleaved by NS3 after overnight incubation with 1 μM enzyme, whereas egl-*EMEG70* (less stable) was cleaved to about 10−20% upon incubation under the same conditions (Figure 4). This observation further supports the idea that inhibition of NS3 by egl-*ELEMS* and even egl-*PEE* is achieved via a classical

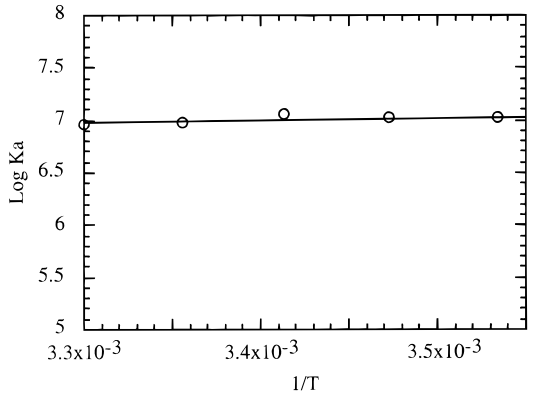

FIGURE 4: Determination of thermodynamic parameters of eglin−proteinase complex formation. Equilibrium association constants were calculated from IC_{50} values as described in the text. Reactions were performed in 50 mM HEPES (pH 7.5), 15% glycerol, 16 μM pep4A, 1% CHAPS, and 30 mM DTT. The pH of the buffer was corrected for the temperature effect on the p*K* value of HEPES. NS3 proteinase at 60, 40, 30, 20, and 15 nM was preincubated at 10, 15, 20, 25, and 30 °C for 15 min with increasing amounts of egl-*ELEMS*. The reaction was started by addition of 10 μM NS4A/4B substrate and stopped after 30 min of incubation by addition of 1% TFA. Cleavage was quantified by RP-HPLC analysis of the samples (mean of duplicate points).

mechanism rather than via substrate competition, as may be the case for the destabilized mutant egl-*EMEG70*.

Next, we checked the specificity of binding for the most potent inhibitors egl-*ELEMS* on HLE and the NS3 proteinase domain (*39*) of the closely related GB-B virus. The serine proteinase HLE is a natural target of eglin c with a K_i of 20 pM. Since its S1 cavity is flexible and can tolerate the C residue in P1 (*32*), which is the case for our eglin inhibitor panel, HLE is a target of choice for establishing inhibitor selectivity. Egl-*ELEMS* does not inhibit the enzyme to any measurable extent up to the maximum concentration tested of 1.6 μM (corresponding to about 10^5 times the K_i value of eglin c for HLE). On the contrary, GBV-B NS3 is inhibited to virtually the same extent as HCV NS3 (30 vs 110 nM). The minimal difference (3.5-fold) can be explained by taking into account different requirements of glycerol concentration for optimal activity of the two proteinases. This is consistent with the fact that the two proteinases have very similar specificities and can recognize each other's substrate, as shown in vitro (*39*).

The N Terminus of Eglin Contributes to Enzyme Binding. Because of an apparent loss of potency shown by the analysis of kinetic parameters obtained in a solid phase assay where eglin was immobilized via its N terminus (data not shown), we wondered whether the N-terminal region of the inhibitor might play a role in binding to the enzyme. To address this issue, we constructed the mutant egl-*EPEMSΔN* by genetically removing the eight N-terminal amino acid residues (including M^1) that have not been observed in X-ray structures of eglin c complexed with several proteinases. These residues are quite flexible, as established both by NMR (*22*) and by X-ray crystallography (*23*) of uncomplexed eglin c. In addition, it is well-established that the absence of these residues does not affect folding of eglin c (*22*, *24*). Although it does not modify the inhibitor's stability [see $T_{m(r)}$, Table 1], removal of the N-terminal fragment affects potency by a factor of 5, indicating that it may contribute to binding the enzyme, possibly by interacting with an exosite-like region

Table 3: N Terminus Mutants of Egl-EPEMS[a]

eglin mutant	N terminal Position								IC_{50} (nM)
	1	2	3	4	5	6	7	8	
egl-*EPEMS*	M	T	E	F	G	S	E	L	184 ± 20
egl-*A2*	M	**A**	E	F	G	S	E	L	194 ± 19
egl-*A4*	M	T	E	**A**	G	S	E	L	230 ± 26
egl-*A6*	M	T	E	F	G	**A**	E	L	260 ± 18
egl-*A6/7*	M	T	E	F	G	**A**	**A**	L	986 ±116
egl-*A7*	M	T	E	F	G	S	**A**	L	650 ± 74
egl-*A8*	M	T	E	F	G	S	E	**A**	220 ± 18
egl-*EPEMSΔN*	Δ	Δ	Δ	Δ	Δ	Δ	Δ	M	1080 ± 96

[a] Amino acid sequences of egl-*EPEMS* variants generated by alanine scanning of the amino terminus and their respective IC_{50} values determined in the NS3 inhibition assay. Alanine substitutions are indicated by shaded cells. Δ indicates a deleted residue.

of the enzyme. To pinpoint the role of individual side chains, we performed an alanine scanning experiment. Mutants of the N-terminal region of egl-*EPEMS* were constructed, purified, and tested on NS3. From this analysis, it appears that residue E^7 is involved in contacting NS3 as shown in Table 3. The double mutant egl-*A6/7* accounts for the 5-fold difference observed with the egl-*EPEMSΔN*.

DISCUSSION

The specificity of proteinases is considered to be predominantly determined by the S1 specificity pocket. In some cases, an inhibitor specificity can be altered simply by mutating the P1 residue (*14*, *30*, *32*). To maintain inhibitory potency and an altered specificity, however, a high complementarity between the inhibitor active site-binding loop and the specificity pockets of the target enzyme is required. According to the standard mechanism of serine proteinase inhibition (*18*), the inhibitor binds to the target proteinase in a substrate-like manner. Contrary to substrates, binding between enzyme and inhibitor is very tight, resulting in k_{cat} and K_m values that are several orders of magnitude lower than those of substrate. A wealth of information has been accumulated in the past 15 years, yet crystallographic studies do not entirely explain the nature of inhibitory potency of proteinaceous serine proteinase inhibitors (*18*, *40*, *41*). In the crystal structures, the scissile bond of inhibitors in complex with proteinases remains intact (*19*), but usually appear distorted toward a tetrahedral intermediate state. A tetrahedral distortion of the carbonyl C center has been reported for all the complexes formed with BPTI, while a distortion of the Michaelis complex toward the tetrahedral intermediate state has not been detected in inhibitors of the Kazal family (*42*, *43*).

Our results with the engineered inhibitors of HCV NS3 proteinase described in this paper are consistent with earlier studies (*31*). They demonstrate that the nature of the P1 side chain is the most crucial factor for specificity and that the binding loop interface must be remodeled to maximize subsite interactions between P5 and P4′ to achieve a reasonable level of inhibition. Each mutation may be regarded as a compromise between optimization of the enzyme inhibitor interface on one hand and maintenance of the crucial contacts between the active site-binding loop and the eglin c "core" on the other. This becomes particularly evident in attempts to introduce P6, P2, and P1′ "NS3 substrate consensus" residues into the corresponding positions of the eglin c active site-binding loop, which compromise the inhibitory potency of the resulting molecules. In fact, T^{44} (P2) and D^{46} (P1′) residues in eglin c are engaged in hydrogen bonds and electrostatic network with the core of the molecule, involving R^{51} and R^{53} (*25*).

The rate constants for association of optimized eglin inhibitors with the NS3 proteinase domain are close to the theoretical limits of diffusion rates in solution (10^7 M^{-1} s^{-1}). These findings suggest that the productive encounter between the eglin inhibitors and the NS3 proteinase is in fact diffusion-controlled. This kinetic behavior parallels the inhibition of HLE (*44*), chymotrypsin, and subtilisin (*45*) by eglin c, which has been reported to occur with second-order rate constants between 10^6 and 10^7 M^{-1} s^{-1}. Eglin c, however, is an inhibitor in the femtomolar range for *S. griseus* proteinases A and B (*14*) and in the picomolar range for HLE and chymotrypsin (*30*), whereas the partial optimization of NS3 eglin inhibitors produces molecules with an affinity that is about 3−4 orders of magnitude weaker. The high affinity of eglin c for a panel of serine proteinases is the result of the very slow dissociation rates of the resulting proteinase−inhibitor complexes, on the order of 10^{-4} s^{-1}. This figure has to be compared to a dissociation rate constant of 0.3−0.9 s^{-1} for the egl-*ELEMS*−NS3 and egl-*EPEMS*−NS3 complexes. A possible explanation for this finding could be the limited complexity of our panel of inhibitors which does not allow a complete sampling of side chain combinations. However, we believe that a more likely explanation resides in the unusual features of the NS3 active site. Although NS3 has a canonical chymotrypsin-like fold, it lacks a series of loops that in other serine proteinases are involved in establishing contacts with substrates or inhibitors (*10*). The optimized NS3 eglin inhibitors might therefore not be able to engage in binding interactions that stabilize other eglin c−proteinase complexes.

A thermodynamic analysis (*46*) has shown that binding of eglin c to serine proteinases is entropy-driven, reflecting the increased degrees of freedom gained by the solvent system when water molecules are removed from both protein surfaces upon binding. We have shown that the same mechanisms are operative in driving NS3−egl-*ELEMS* complex formation, since the associated entropy gain was the main driving force of the process. When we attempted to introduce hydrophobic residues (derived from the NS5A/5B cleavage site) with the aim of modulating the off rate by increasing the lipophilicity of the interface, we obtained poorer inhibitors (egl-*W*, egl-*WMS*, egl-*ELI*, and egl-*YWMS*). In conclusion, conformational constraints appear to be crucial to the free energy change of eglin−proteinase complex formation by limiting the entropy loss associated with complexation. The potency of the egl-*ELE* should in fact be compared to that of the pentapeptide spanning P1−P5 (>1 mM), which is 3−4 orders of magnitude higher (*47*). It is very likely that this difference is mainly due to the (preorganized) backbone conformation of the macromolecule inhibitor versus the unconstrained pentapeptide.

The crystal structure of eglin c is known from its complexes with various serine proteinases (*24*−*28*). In

[3] Our unpublished observations.

addition, the structure of free eglin c was resolved at 1.95 Å resolution (*23*) and the final model contains all 70 amino acids. In comparison to the eglin structure known from its complexes with proteinases, only small differences have been observed in free eglin c. However, the active site-binding loop and a few residues on the surface of eglin c have been found in different conformations due to crystal contacts. In contrast to the eglin c present in complexed structures, the first seven amino acids of the highly flexible amino terminus could be located. The deletion of the N terminus of egl-*EPEMS* (egl-*EPEMS*Δ*N*) and the alanine scanning mutants suggest that E^7 is involved in binding to the enzyme, albeit with a small energetic contribution. We do not know if this is a more general phenomenon that applies to other eglin c− or CI-2−proteinase complexes. The N terminus of these two inhibitors does not contribute to the thermodynamic stability [see $T_{m(r)}$ values] and folding properties of the proteins as established by X-ray crystallography (*24*−*28*). However, binding affinity measurements of N-deleted inhibitors have not been reported. It may be argued that the involvement of the N terminus of eglin c in binding the enzyme is artifactual because NS3 is a truncation of a larger protein, but experimental evidence[3] suggests that binding to the full-length NS3 enzyme also is affected by the presence of the N terminus.

The design of selective inhibitors of HCV NS3 proteinase based on eglin c reported here offers a unique opportunity to evaluate the requirements for effective inhibition of NS3 enzymatic activity. It is worth noting that because of its size and lack of disulfides, eglin c is readily amenable to chemical synthesis approaches (*48*) and thus offers the opportunity to explore the activity of non-natural amino acids at selected positions within the active site-binding loop. In conclusion, these results support the expectation that designing small molecules that are reversible and competitive inhibitors of NS3 is fraught with difficulties. We are attempting to cocrystallize one of our most potent inhibitors and hope to be able to provide clues to medicinal chemists to accelerate the quest for potent small molecule inhibitors.

ACKNOWLEDGMENT

We are grateful to R. Cortese for continuous support and valuable discussions, V. G. Matassa for critically reviewing the manuscript, S. Altamura for help with the HLE assay, A. Pessi and S. Acali for peptide synthesis, F. Bonelli for assistance with mass spectrometry analysis, C. Traboni for providing the GBV-B NS3 proteinase, G. Biasiol for providing purified HCV NS3, and B. McManus and J. Clench for revision of the manuscript.

REFERENCES

1. Choo, Q. L., Kuo, G., Weiner, A. J., Overby, L. R., Bradley, D. W., and Houghton, M. (1989) *Science 244*, 359−362.
2. Kuo, G., Choo, Q. L., Alter, H. J., Gitnick, G. L., Redecker, A. G., Purcell, R. H., Myamura, T., Dienstag, J. L., Alter, M. J., Syevens, C. E., Tagtmeyer, G. E., Bonino, F., Colombo, M., Lee, W. S., Kuo, C., Berger, K., Shister, J. R., Overby, L. R., Bradley, D. W., and Houghton M. (1989) *Science 244*, 362−364.
3. Chien, D., Choo, Q. L., Tabrizi, A., Kuo, C., McFarland, J., Berger, K., Lee, C., Shuster, J., Nguyen, T., Moyer, D., Tong, M. M., Furuta, S., Omata, M., Tegtmeyer, G., Alter, H., Schiff, E., Jeffers, L., Houghton, M., and Kuo, G. (1992) *Proc. Natl. Acad. Sci. U.S.A. 89*, 10011−10015.
4. Weiland, O. (1994) *FEMS Microbiol. Rev. 14*, 279−288.
5. Neddermann, P., Tomei, L., Steinkühler, C., Gallinari, P., Tramontano, A., and De Francesco, R. (1997) *Biol. Chem. Hoppe-Seyler 378*, 469−476.
6. Pizzi, E., Tramontano, A., Tomei, L., La Monica, N., Failla, C., Sardana, M., Wood, T., and De Francesco, R. (1994) *Proc. Natl. Acad. Sci. U.S.A. 91*, 888−892.
7. Bartenschlager, R., Ahlborn-Laake, L., Mous, J., and Jacobsen, H. (1994) *J. Virol. 68*, 5045−5055.
8. Failla, C., Tomei, L., and De Francesco, R. (1994) *J. Virol. 68*, 3753−3760.
9. Lin, C., Pragai, B. M., Grakoui, A., Xu, J., and Rice, C. M. (1994) *J. Virol. 68*, 8147−8157.
10. Kim, J. L., Morgenstern, K. A., Lin, C., Fox, T., Dwyer, M. D., Landro, J. A., Chambers, S. P., Markland, W., Lepre, C. A., O'Malley, E. T., Harbeson, S. L., Rice, C. M., Murcko, M. A., Caron, P. R., and Thomson, J. A. (1996) *Cell 87*, 343−355.
11. Love, R. A., Parge, H. E., Wickersham, J. A., Hostomsky, Z., Habuka, N., Moomaw, E. W., Adachi, T., and Hostomska, Z. (1996) *Cell 87*, 331−342.
12. Martin, F., Volpari, C., Steinkühler, C., Dimasi, N., Brunetti, M., Biasiol, G., Altamura, S., Cortese, R., De Francesco, R., and Sollazzo, M. (1997) *Protein Eng. 10*, 607−614.
13. Dimasi, N., Martin, F., Volpari, C., Brunetti, M., Biasiol, G., Altamura, S., Cortese, R., De Francesco, R., Steinkühler, C., and Sollazzo, M. (1997) *J. Virol. 71*, 7461−7469.
14. Qasim, M. A., Ganz, P. J., Saunders, C. W., Bateman, K. S., James, M. N., and Laskowski, M., Jr. (1997) *Biochemistry 36*, 1598−1607.
15. Seemüller, U., Eulitz, M., Fritz, H., and Strobl, A. (1980) *Physiol. Chem. Hoppe-Seyler 361*, 1841−1846.
16. Rink, A., Liersch, M., Sieber, P., and Meyer, F. (1984) *Nucleic Acids Res. 12*, 6369−6387.
17. Veiko, V. P., Osipov, A. S., Shekhter, I. L., Bulenkov, M. T., Ratmanova, K. I., Gul'ko, L. B., Chibiskova, N. A., Erreis, L. L., Derevshchikova, E. B., and Debabov, V. G. (1995) *Russ. J. Bioorg. Chem. 21*, 303−306.
18. Laskowski, M., Jr., and Kato, I. (1980) *Annu. Rev. Biochem. 49*, 593−626.
19. Bode, W., and Huber, R. (1992) *Eur. J. Biochem. 204*, 433−451.
20. Creighton, T. E., Bagley, C. J., Cooper, L., Darby, N. J., Freedman, R. B., Kemmink, J., and Sheikh, A. (1993) *J. Mol. Biol. 232*, 1176−1196.
21. McPhalen, C. A., and James, M. N. G. (1988) *Biochemistry 27*, 6582−6598.
22. Hyberts, S. G., Goldberg, M. S., Havel, T. F., and Wagner, G. (1992) *Protein Sci. 1*, 736−751.
23. Hipler, K., Priestle, J. P., Rahuel, J., and Grütter, M. G. (1992) *FEBS Lett. 309*, 139−145.
24. McPhalen, C. A., Schnebli, H. P., and James, M. N. G. (1985) *FEBS Lett. 188*, 55−58.
25. Bode, W., Papamokos, E., Musil, D., Seemüller, U., and Fritz, H. (1986) *EMBO J. 5*, 813−818.
26. Heinz, D. W., Priestle, J. P., Rahuel, J., Wilson, K. S., and Grütter, M. G. (1991) *J. Mol. Biol. 217*, 353−371.
27. Mcphalen, C. A., Svendsen, I., Jonassen, I., and James, M. N. G. (1985) *Proc. Natl. Acad. Sci. U.S.A. 82*, 7242−7246.
28. Frigerio, F., Coda, A., Pugliese, L., Lionetti, C., Menegatti, E., Amiconi, G., Schnebli, H. P., Ascenzi, P., and Bolognesi, M. (1992) *J. Mol. Biol. 225*, 107−123.
29. Gros, P., Teplyakov, A. V., and Hol, W. (1992*) Proteins: Struct., Funct., Genet. 12*, 63−74.
30. Hipler, K., Priestle, J. P., Rahuel, J., and Grütter, M. G. (1996) *Adv. Exp. Med. Biol. 379*, 43−47.
31. Heinz, D. W., Hyberts, S., Peng, J. W., Priestle, J. P., Wagner, G., and Grütter, M. G. (1992) *Biochemistry 31*, 8755−8766.
32. Lu, W., Apostol, I., Qasim, M. A., Warne, N., Wynn, R., Zhang, W. L., Anderson, S., Chiang, Y. W., Ogin, E., Rothberg, I., Ryan, K., and Laskowski, M., Jr. (1997) *J. Mol. Biol. 266*, 441−461.

33. De Francesco, R., Urbani, A., Nardi, M. C., Tomei, L., Steinkühler, C., and Tramontano, A. (1996) *Biochemistry 35*, 13282−13287.
34. Taliani, M., Bianchi, E., Narjes, F., Fossatelli, M., Urbani, A., Steinkühler, C., De Francesco, R., and Pessi, A. (1996) *Anal. Biochem. 240*, 60−67.
35. Urbani, A., Bianchi, E., Narjes, F., Tramontano, A., De Francesco, R., Steinkühler, C., and Pessi, A. (1997) *J. Biol. Chem. 272*, 9204−9209.
36. Holmes, D. I. R., Mantafounis, D., Ward, W. H. J., and Leatherbarrow, R. J. (1996) *Protein Pept. Lett. 3*, 415−422.
37. Landro, J. A., Raybuck, S. A., Luong, Y. P., O'Malley, E. T., Harbeson, L. S., Morgenstern, K. A., Rao, G., and Livingston, D. J. (1997) *Biochemistry 36*, 9340−9348.
38. Braun, N. J., Bodmer, J. L., Virca, G. D., Metz-Virca, G., Masheler, R., Bieth, J. G., and Schnebli, H. P. (1987) *Biol. Chem. Hoppe-Seyler 368*, 299−308.
39. Scarselli, E., Urbani, A., Sbardellati, A., Tomei, L., De Francesco, R., and Traboni, C. (1997) *J. Virol. 71*, 4985−4989.
40. Estell, D. A., Wilson, K. A., and Laskowski, M., Jr. (1980) *Biochemistry 19*, 131−137.
41. Estell, D. A., and Laskowski, M., Jr. (1980) *Biochemistry 19*, 124−131.
42. Marquat, M., Walter, J., Deisenhofer, J., Bode, W., and Huber, R. (1983) *Acta Crystallogr. B39*, 480−490.
43. Read, R. J., and James, M. N. G. (1986) in *Proteinase Inhibitors* (Barrett, A. J., and Salvesen, G., Eds.) pp 301−336, Elsevier, Amsterdam.
44. Baici, A., and Seemüller, U. (1984) *Biochem. J. 218*, 829−833.
45. Ascenzi, P., Amiconi, G., Menegatti, E., Guarneri, M., Bolognesi, M., and Schnebli, H. P. (1988) *J. Enzyme Inhib. 2*, 167−172.
46. Ascenzi, P., Aducci, P., Amiconi, G., Ballio, A., Guaragna, A., Menegatti, E., Schnebli, H. P., and Bolognesi, M. (1991) *J. Mol. Recognit. 4*, 113−119.
47. Ingallinella, P., Altamura, S., Bianchi, E., Taliani, M., Ingenito, R., Cortese, R., De Francesco, R., Steinkühler, C., and Pessi, A. (1998) *Biochemistry 37*, 8906−8914.
48. Schnolzer, M., and Kent, S. B. H. (1992) *Science 256*, 221−225.

BI980283W